Rounded lateral habits of polyethylene single crystals

A. Toda
Department of Physics, Faculty of Science, Kyoto University, Kyoto 606, Japan
(Received 30 January 1990; revised 12 March 1990; accepted 14 March 1990)

The lateral crystal habit of polyethylene has been studied experimentally and theoretically. When the fraction of low-molecular-weight polyethylene ($M_w = 2000$ and $M_w/M_n = 1.1$) is crystallized from n-hexacontane solution at high temperatures ($T > 105°C$), most chains are extended in the crystals and the lateral shape of single crystals becomes lenticular. The longer axis of the lenticular profile is parallel to the b axis of crystals and the tip has an acute angle; the {1 1 0} growth face disappears in this habit. The curved outline of the lenticular habit has been analysed with the kinetic theory of Seto and Frank on the basis of nucleation-controlled growth. A moving boundary condition has been applied to the growth of the crystal sector, as was done by Mansfield. It is shown that the lenticular habit is expected for strongly retarded crystallization on the {2 0 0} growth face.

(Keywords: polyethylene; single crystal; crystallization; crystal habit; kinetics)

INTRODUCTION

Polyethylene single crystals with well faceted lateral habits can be obtained from dilute solutions at relatively low crystallization temperatures[1,2]; they are in the shape of a lozenge with {1 1 0} growth face (*Figure 1a*) or a truncated lozenge with {1 1 0} and {2 0 0} growth faces (*Figure 1b*). At higher crystallization temperatures ($T >$ 100°C), the profile of the growth front of the {2 0 0} sector becomes rounded and the truncation becomes larger, as shown in *Figures 1c* and *1d*[3]. Several authors have studied the mechanism of rounding of crystal habits in recent years[4–8] and this is still the subject of controversy.

Two types of mechanism have been proposed for the rounding of habits. (1) In the first model, it is suggested[5] that the growth face can be thermally roughened; namely the free energy of a step (*Figure 2*) vanishes at high temperatures[9] and steps can be generated without the activated state of secondary nucleation. Under such a condition, crystal growth becomes isotropic and the profile of the growth front becomes rounded. (2) It is assumed in the other model[6–8] that the advance of steps is interrupted by impurities[6] or lattice strain[8]. This effect results in the accumulation of steps on the growth face and the rounding of the growth front. It should be noted that secondary (two-dimensional) nucleation controls crystal growth in the latter model, while crystallization on a thermally roughened surface is not limited by the nucleation process.

For crystals obtained at high temperatures, we must also explain the strong anisotropy, i.e. large axial ratio, of habits shown in *Figures 1c* and *1d*. (1) In the first model, the anisotropy cannot be explained at all by thermal roughening. When the growth face is thermally roughened, the face can grow without secondary nucleation and growth should be enhanced. Observed habits show just the opposite; the rounded growth front of the {2 0 0} sector grows very slowly compared to the flat front of the {1 1 0} sector. (2) With the assumption of interrupted crystallization, it is proper to expect retarded growth of the rounded face. I support this hypothesis because it simultaneously explains curved lateral habits and the anisotropy of habits.

In the present paper, rounded lateral habits are analysed with model (2) on the basis of nucleation-controlled growth. First, we discuss experimental results on the lateral habits of low-molecular-weight polyethylene crystallized from alkane solution at high temperatures. The observed habits show different kinds of morphology from those shown in *Figure 1*. Secondly, we discuss a kinetic model based on a recent study by Mansfield[7]. With the assumption of retarded movement of steps, he calculated the curved profile of single crystals; the profile is similar to the lateral shape of the single crystal shown in *Figure 1c*. We extend his theoretical treatment in order to explain the distinct habits observed in the present experiments. Thirdly, we analyse the experimental results with the kinetic theory.

EXPERIMENTS AND RESULTS

The low-molecular-weight fraction of polyethylene (Polymer Laboratories) has the following average molecular weight: $M_w = 2000$ and $M_w/M_n = 1.1$. As the solvent, n-hexacontane ($C_{60}H_{122}$, Fluka) was used. Experiments were performed in the following manner. The components of the mixture were weighed out in the desired ratio and allowed to mix in n-octane solution at 130°C. The solution was poured onto a carbon film evaporated on mica, which was placed on a hot plate ($T \sim 70°C$) in order to evaporate n-octane. The film (several tens of micrometres thick) was then melted on a Mettler hot stage at 130°C for 3 min, quenched to the crystallization temperature ($T = 104$–$112°C$) and crystallized isothermally. After the desired crystallization period, the mica was immersed in hot n-octane at about 75°C in

0032-3861/91/050771-10

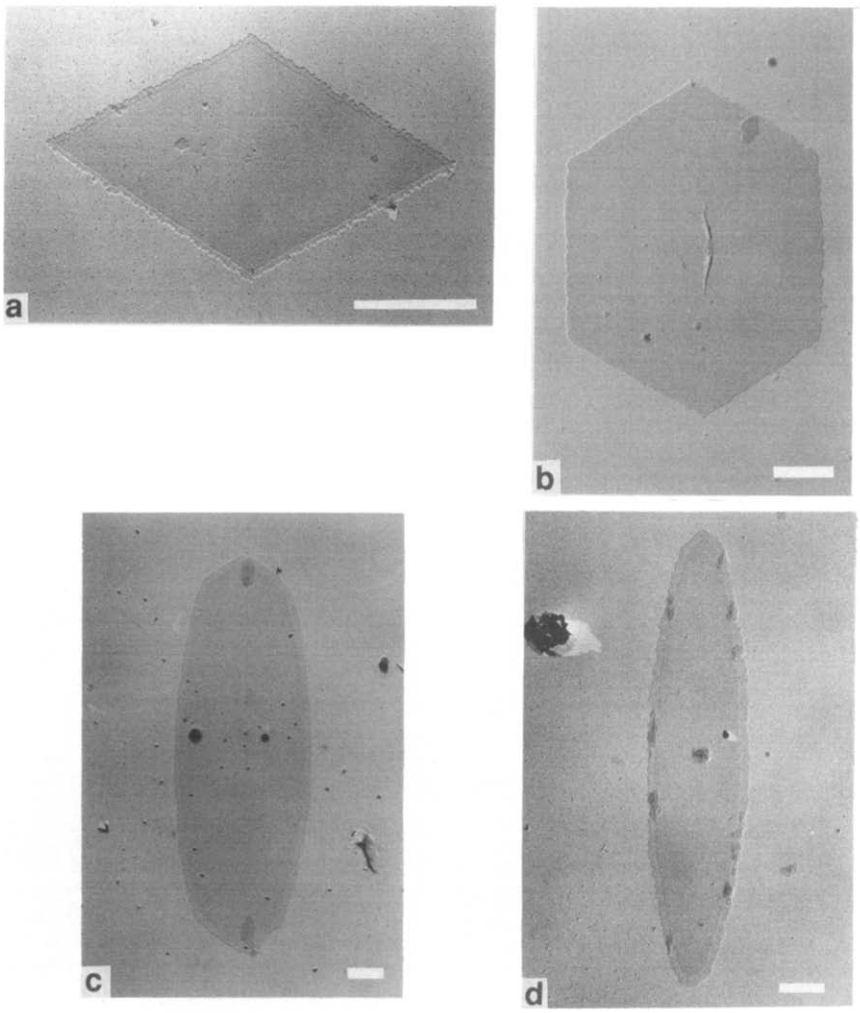

Figure 1 Electron micrographs of single crystals ($M_w = 1.1 \times 10^4$ and $M_w/M_n = 1.16$) grown from (a) 2.5×10^{-5}% xylene solution at 73.3°C, (b) 0.01% n-octane solution at 98.0°C, (c) 0.02% diphenyl ether solution at 114°C and (d) 0.1% n-dotriacontane solution at 110°C. The *b* axis of crystals is vertical. All are shadowed with Pt–Pd. Bar lines represent 1 μm

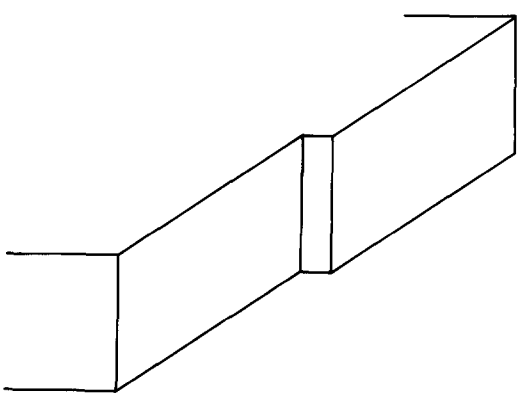

Figure 2 Schematic representation of a step on the lateral face of single crystals. Crystallization at the step creates no additional lateral surface and does not require the excess free energy of lateral surface

order to remove the solution, the uncrystallized portion of polyethylene at the time of sampling and the solvent, n-hexacontane. Then, the sample on carbon film was examined by electron microscopy.

Figure 3 shows the lateral habits of single crystals obtained at several crystallization temperatures. From the shadowing length, the thickness of lamellae is estimated to be about 250 Å irrespective of temperature; most chains are supposed to be extended in the crystals, considering the average molecular weight and the distribution. The observed growth fronts are curved and the axial ratio (length along *b* axis/length along *a* axis) is very high, 3–15. The profiles shown in *Figures 3b–d* are curved in the central region and almost linear near the tips. The outline has an acute angle at the tips, and there is no evidence of the {1 1 0} growth face. We call these habits lenticular habits. The habits are similar to those of melt-crystallized polyethylene of higher molecular weight; they have been reported by several authors recently[10–13].

In the temperature range 108.8–110.5°C, two types of lateral habits with distinct axial ratio as shown in *Figures 3c* and *3d* have been observed simultaneously. While the crystals shown in *Figure 3c* are frequently gathered together on the substrate, the crystals shown in *Figure 3d* are usually scattered one by one on the same substrate. This difference in morphology will be due to molecular-weight fractionation, which is unavoidable at low supercoolings. In the region where the density of crystals is high, the supply of higher-molecular-weight component is not enough, so that the impurity effect caused by lower-molecular-weight component will be the main reason for the distinct habit in the crowded region; the

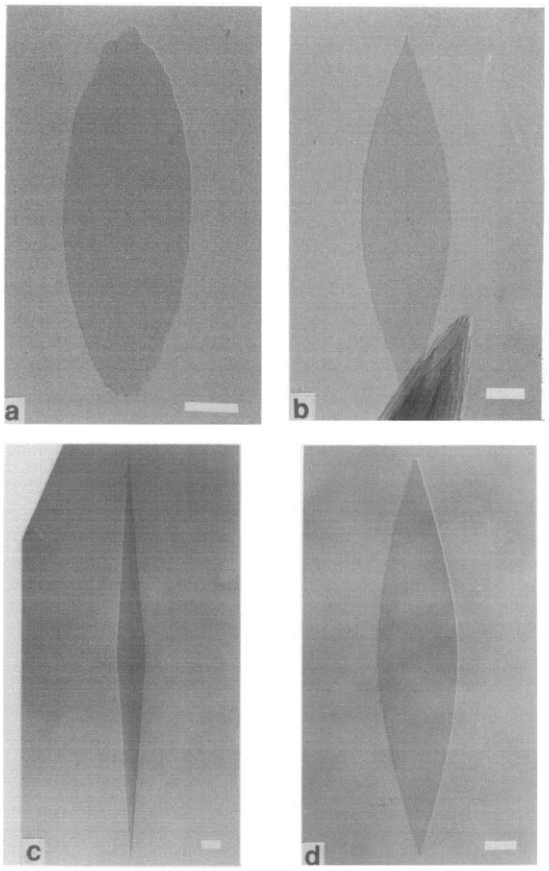

Figure 3 Electron micrographs of single crystals ($M_w = 2000$) grown from 17% n-hexacontane solution at (a) 104°C, (b) 106°C, (c) 110.5°C and (d) 112°C. The b axis of crystals is vertical. All are shadowed with Pt–Pd. Bar lines represent 1 μm

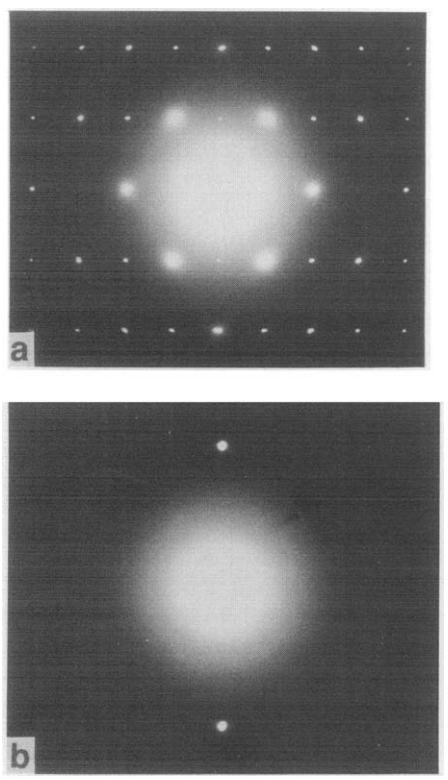

Figure 4 Electron diffraction patterns of single crystals ($M_w = 2000$) grown from 17% n-hexacontane solution at (a) 104°C and (b) 110.5°C. The b^* axis is vertical

detailed mechanism of the effect will be discussed in the section on the application of the kinetic model.

Figure 4 shows electron diffraction patterns. From the patterns, it can be seen that chains in the crystals are almost perpendicular to the substrate at lower temperatures (*Figure 4a*), but they are inclined in the direction of the a axis at higher temperatures (*Figure 4b*). The sense of chain tilting should be identical throughout a given crystal because the patterns of both growth and dissolution of overgrown crystals in *Figure 5* are asymmetric between opposite lateral faces; overgrowth occurred while the samples were immersed in hot n-octane in order to remove the solution. These behaviours of chain tilting have been confirmed for the folded-chain crystals of higher-molecular-weight polyethylene crystallized at higher temperatures[12–14]. It is also known for alkane crystals that chains are tilted with respect to the plane of the end-group in higher-temperature phases such as C and D (rotator) phases[15]. It is thought that the tilting is due to the thermal motion of chain ends and the resultant defect structures in the plane of the end-group. In the present case, extended chains are inclined at higher temperatures, and this fact may suggest that the crystals are rather disordered like alkane crystals in the high-temperature phases.

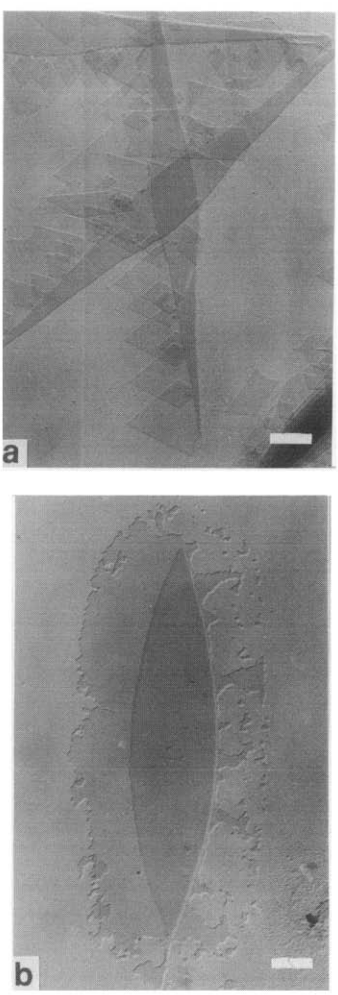

Figure 5 Electron micrographs of single crystals ($M_w = 2000$) grown from n-hexacontane solution at (a) 10%, 109°C and (b) 30%, 114°C. The patterns of (a) growth and (b) dissolution of overgrown crystals are asymmetric between opposite lateral faces. All are shadowed with Pt–Pd. Bar lines represent 1 μm

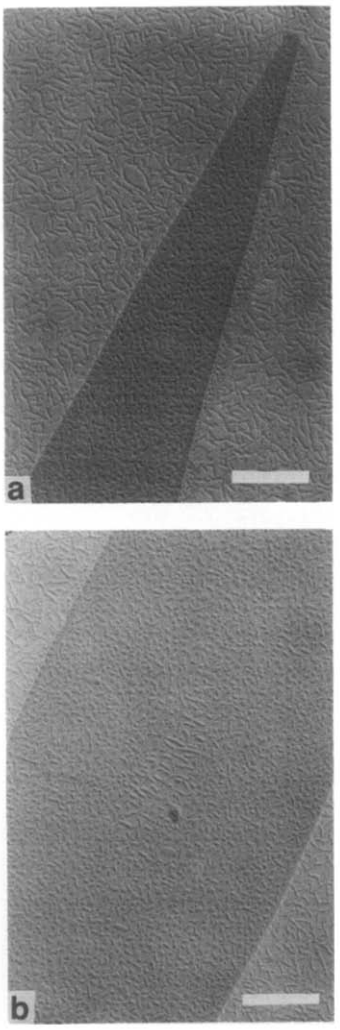

Figure 6 Electron micrographs of single crystals ($M_w = 2000$) grown from 17% n-hexacontane solution at 111°C. Specimens are decorated with evaporated polyethylene by the method of Wittmann and Lotz and shadowed with Pt–Pd. Bar lines represent 0.5 μm.

Figure 6 shows the crystals decorated with evaporated polyethylene by Wittmann and Lotz's method[16]. The decoration as a whole does not show any orientation pattern and this fact means that the lamellar surface is rather disordered in comparison with alkane and polyethylene single crystals with well faceted lateral habits. It can also be seen that the pattern shows orientation in the direction of the *a* axis within a small region around the centre of crystals in *Figure 6b*. The evidence suggests that the higher-molecular-weight component crystallizes at the initial stage of growth and the chains are folded in a comparatively regular manner within this region.

Figures 7a and *7b* show the lateral habits of {3 1 0} and {1 1 0} twins, respectively. It is seen that growth is enhanced at the re-entrant corner of the {3 1 0} twin but not at the corner of the {1 1 0} twin. The difference will be due to the fact that the angle at the re-entrant corner of the {3 1 0} twin is smaller than that of the {1 1 0} twin; namely crystallization will be easier at the corner of the {3 1 0} twin compared to that of the {1 1 0} twin. Enhanced growth at the re-entrant corner of {3 1 0} twins means that, on normal faces, a step has an advantage over a flat surface in crystallization; the free energy of steps does not vanish and the growth face is not completely thermally roughened.

Linear growth rates of single crystals were determined from the change in crystal size with crystallization period. Since a self-seeding method[17] was not utilized, there was a distribution of crystal size. It was assumed that the maximum size of crystals represented the size at the time of sampling. The size increased linearly with time in the initial stage. *Figure 8* shows the dependence of growth rate on crystallization temperature at a constant concentration. Plots of growth rates along the *a* axis are split into two branches (● and ▲ in *Figure 8*) in the temperature range 108.8–110.5°C. These branches (▲ and ●) correspond to the lateral habits shown in *Figures 3c* and *3d*, respectively. Growth rates in both directions of *a* and *b* axes decrease exponentially as the temperature increases. Since the sample has a molecular-weight distribution and the dissolution temperature of the low-molecular-weight fraction depends strongly on the molecular weight[18], definite supercooling cannot be determined in the present experiments. *Figure 9* shows the d.s.c. thermogram. The dissolution peak is at about 115°C, but the endotherm is rather broad. From the comparison of melting endotherms of pure polyethylene ($M_w = 2000$) and n-hexacontane, we can see the broad distribution of melting points of the fraction.

In order to analyse the growth kinetics in the following discussion, the tangent of the angle made by the outline of crystals at tips, tan θ, was measured, and is shown in *Figure 10* with the ratio of growth rates, G_a/G_b, as a function of crystallization temperature.

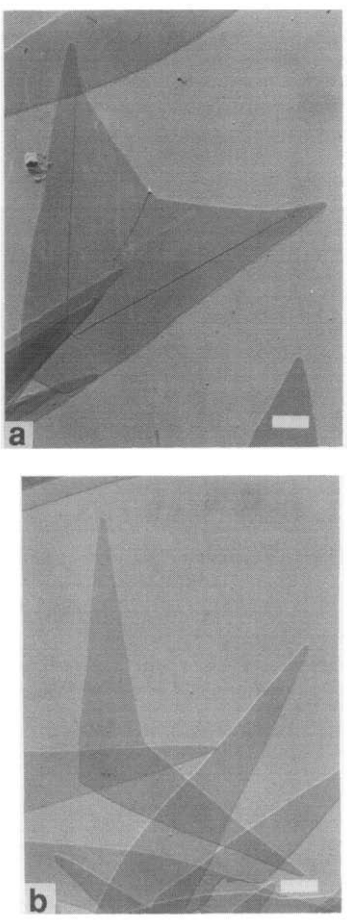

Figure 7 Electron micrographs of (a) {3 1 0} and (b) {1 1 0} twins ($M_w = 2000$) grown from 17% n-hexacontane solution at 111°C. Specimens are decorated with evaporated polyethylene by the method of Wittmann and Lotz and shadowed with Pt–Pd. Bar lines represent 1 μm

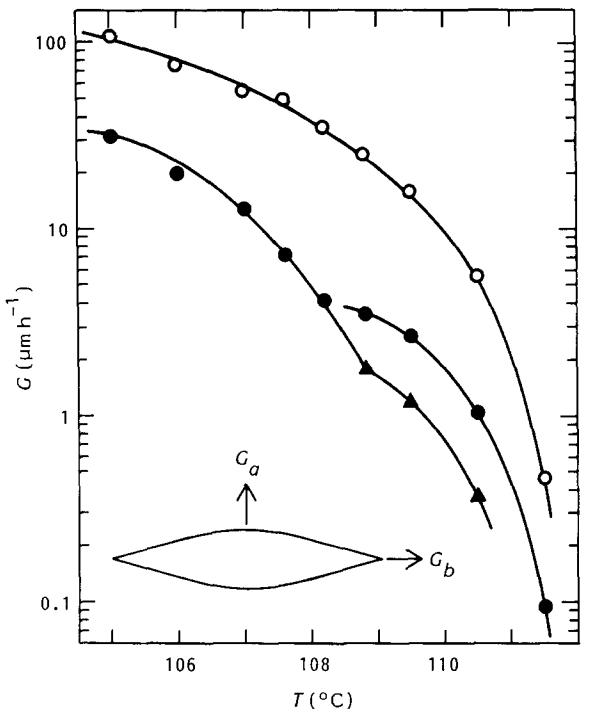

Figure 8 Temperature dependence of linear growth rates along *a* and *b* axes, G_a (●, ▲), and G_b (○), of single crystals ($M_w = 2000$) grown from 17% n-hexacontane solution. $G_a/G_b \sim \tan\theta$ for ▲

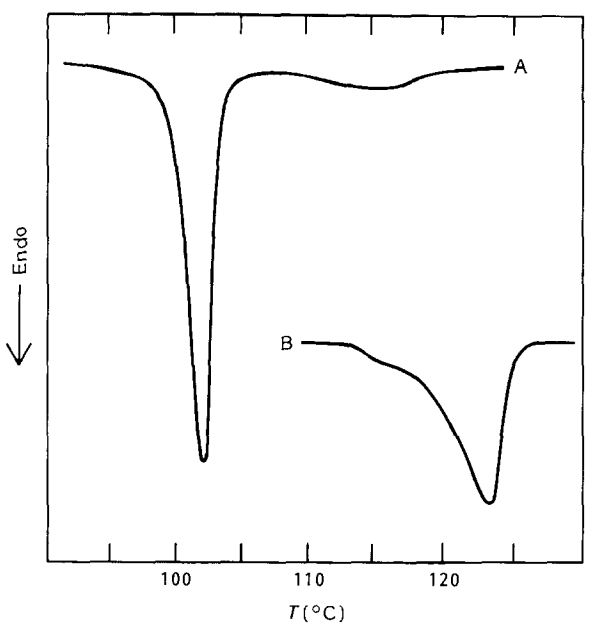

Figure 9 D.s.c. curves of (A) 17% n-hexacontane solution of polyethylene ($M_w = 2000$) and (B) pure polyethylene ($M_w = 2000$).Heating rate is 5°C min^{-1}

KINETIC MODEL

Under the condition of nucleation-controlled growth, the process of crystallization is considered as the following sequence. New stems appear on a flat substrate at a nucleation rate *ia* per site (*a* is the width of a site); this stem forms a pair of steps facing in opposite directions on the substrate. Subsequent stems lay down laterally next to the first stem at a rate v/a; the process can be treated as the advance of steps at a velocity v. It is not well understood whether nucleation includes the formation of single or several stems on the substrate, namely what is the critical nucleus[19], but this fact has no influence on the following discussion. Since steps move laterally left or right, the substrate can be considered to be one-dimensional and steps are treated as kinks on the one-dimensional substrate (*Figure 11*). In order to calculate the growth rate of crystals, we must consider the kinetics of steps generated by different nucleation events, namely the processes of generation, movement and annihilation of kinks and anti-kinks. Kinetic equations that account for such processes were proposed by Seto[20] and Frank[21]. The growth rate was obtained as a function of i and v, and the profile of the growth front was proved to be almost flat[21]; the result was consistent with the assumption of nucleation-controlled growth. However, I have shown that the profile can be curved, when the movement of steps is completely interrupted and the steps are accumulated on the growth face[6].

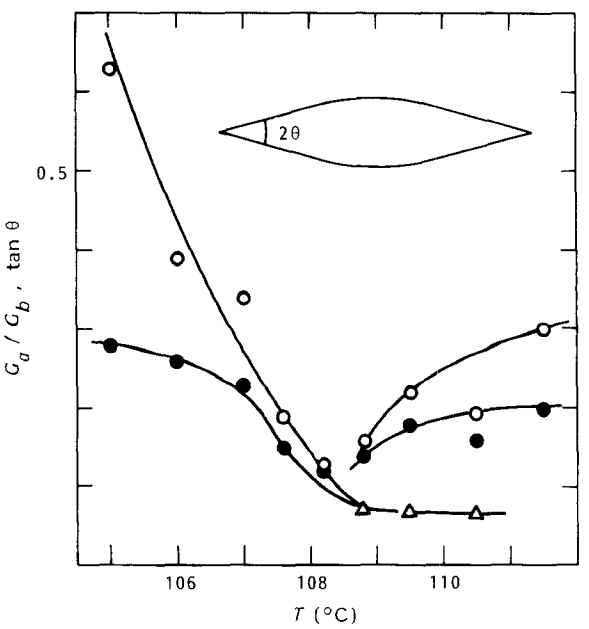

Figure 10 Temperature dependence of the tangent of angle at the tips, tan θ (○, △), and the ratio of growth rate, G_a/G_b (●, △), of single crystals ($M_w = 2000$) grown from 17% n-hexacontane solution. $G_a/G_b \sim \tan\theta$ for △

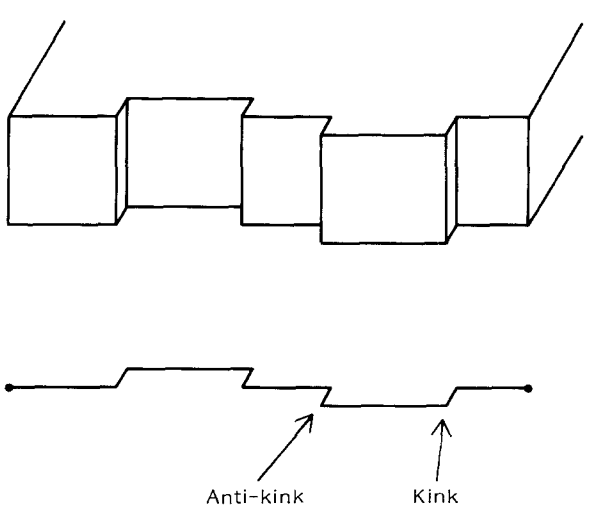

Figure 11 Correspondence between steps on growth face and kinks on one-dimensional substrate

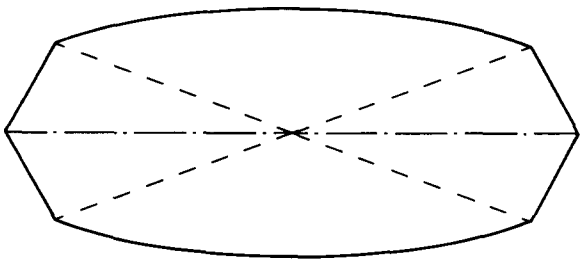

Figure 12 Schematic representation of typical habit predicted by Mansfield

In a recent study by Mansfield[7], it has been suggested that the profile can also be rounded if the advance of steps is only retarded. With this assumption, he predicted the habits shown in *Figure 12* from the kinetic theory of Seto and Frank. While it has been assumed in preceding studies that the boundary of the one-dimensional substrate does not move, he considered the effect of spreading of {2 0 0} sectors during crystal growth, namely the effect of advancing boundaries on the kinetics of kinks. He has shown that the profile of the growth front of the {2 0 0} sector becomes part of an ellipse, when the advance of steps on the {2 0 0} face becomes as slow as that of sector boundaries. Since the advance of steps is expected to be much faster than that of sector boundaries on the basis of standard nucleation theory, the advance of steps on the {2 0 0} growth face should be interrupted, irrespective of the cause of interruption. The predicted profile in *Figure 12* just corresponds to the lateral habits of polyethylene crystallized at relatively high temperatures; the habits are composed of a straight growth front in {1 1 0} sectors and a curved one in {2 0 0} sectors.

The crystals obtained in the present experiments show the distinct type of morphology, lenticular habit (*Figures 3b–d*), in which tips have an acute angle and {1 1 0} sectors disappear. The disappearance of the {1 1 0} sector can be explained if the advance of steps on the {2 0 0} face becomes slower than that of sector boundaries. Since the steps on the {2 0 0} face cannot reach the boundaries under such a condition, the initial layer of substrate will never be completed and the sector boundaries move parallel to the *b* axis[7]. Therefore, the initial width of {1 1 0} sectors remains constant during crystal growth, while curved {2 0 0} growth fronts spread. If the width is narrow enough, it is probable that the {1 1 0} growth front cannot be recognized experimentally owing to overgrowth at the tips or to the coarseness of shadowing contrast of electron micrographs. We present an analytical treatment in order to calculate the curved profile of the {2 0 0} growth face under the condition that the advance of steps is slower than that of sector boundaries.

Seto[20] and Frank[21] proposed differential equations that represented the kinetics of kinks and anti-kinks on a one-dimensional substrate:

$$\frac{\partial r}{\partial t} + v\frac{\partial r}{\partial x} = -2vrl + i \tag{1a}$$

$$\frac{\partial l}{\partial t} - v\frac{\partial l}{\partial x} = -2vrl + i \tag{1b}$$

where $r(x, t)$ and $l(x, t)$ are the densities of kinks and anti-kinks that are travelling to the right (positive x direction) and left, respectively, at velocity v. The left-hand sides of the equations represent the uniform translation of (anti-)kinks with velocity $\pm v$. The term $-2vrl$ represents the rate of annihilation of kinks and anti-kinks by collisions with each other, and the term i represents the rate of pairwise formation of kink and anti-kink by nucleation. We assume that the width of the substrate increases at a velocity h in both directions. Since no steps enter from the outside of the limits $x = \pm ht$, the boundary conditions are:

$$r(-ht, t) = 0 \tag{2a}$$

$$l(ht, t) = 0 \tag{2b}$$

For $h < v$, Mansfield has proved that the solution gives an elliptical outline of growth front and the crystal habits shown in *Figure 12* can be expected[7]. We discuss the solution for $h > v$. Additional boundary conditions should be satisfied for $h > v$ because kinks and anti-kinks cannot reach the boundaries from inside, too:

$$r(ht, t) = 0 \tag{3a}$$

$$l(-ht, t) = 0 \tag{3b}$$

The symmetry relation:

$$r(x, t) = l(-x, t) \tag{4}$$

holds for the solution.

In the following discussion, we solve equations (1) within each region shown in *Figure 13*, separately.

Region A, $vt < x < ht$

Equations (1) are first-order partial differential equations of r and l with respect to two independent variables, x and t. The differential of r can be expressed as:

$$\mathrm{d}r = \frac{\partial r}{\partial t}\mathrm{d}t + \frac{\partial r}{\partial x}\mathrm{d}x$$

On a characteristic line, $x = vt + C_1$ (C_1 is a constant), in space–time representation, we have the following differential equation of r from equation (1a) and relation $\mathrm{d}x = v\,\mathrm{d}t$:

$$\frac{\mathrm{d}r}{\mathrm{d}t} = \frac{\partial r}{\partial t} + v\frac{\partial r}{\partial x} = -2vrl + i$$

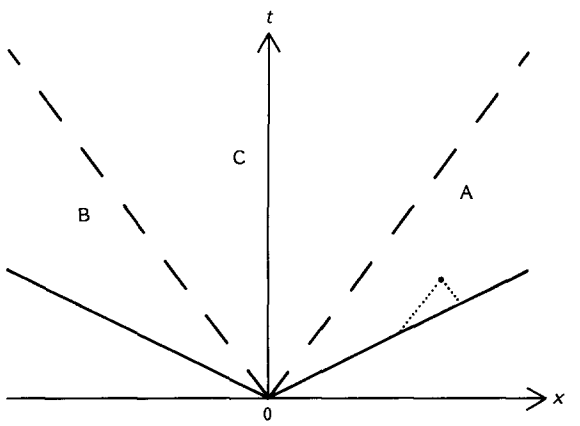

Figure 13 Space–time representation of boundaries of substrate $x = \pm ht$ (full lines). The region $-ht < x < ht$ is divided into three regions, A, B and C, by broken lines, $x = \pm vt$. At a point in region A, the solutions for r and l can be obtained by the integration of equations (5) along dotted lines from the boundary $x = ht$

so that:

$$r = \int_{x=vt+C_1} (-2vrl + i)\,dt \tag{5a}$$

On another characteristic line, $x = -vt + C_2$ (C_2 is another constant), we have:

$$l = \int_{x=-vt+C_2} (-2vrl + i)\,dt \tag{5b}$$

In region A, the solutions of r and l can be obtained by the integration of equations (5) from the boundary $x = ht$ (*Figure 13*). Since the values of r and l are constant (zero) on the boundary (equations (2b) and (3a)), the solutions are identical at any point on a line $x = ht + C_3$ (C_3 is a constant); solutions at a point x are only dependent on the distance from the boundary $ht - x$. Therefore, differentials dr and dl should be zero on this line. Owing to the fact that $dr = dl = 0$ and $dx = h\,dt$, which hold on this line, the solutions of r and l satisfy:

$$\frac{\partial r}{\partial t} + h\frac{\partial r}{\partial x} = 0 \tag{6a}$$

$$\frac{\partial l}{\partial t} + h\frac{\partial l}{\partial x} = 0 \tag{6b}$$

From equations (1) and (6), we have:

$$(v-h)\frac{dr}{dx} = -2vrl + i \tag{7a}$$

$$-(v+h)\frac{dl}{dx} = -2vrl + i \tag{7b}$$

at a definite time t_0. Apparently, the following relation holds:

$$(v-h)\,dr = -(v+h)\,dl$$

which implies:

$$l = \frac{h-v}{h+v}r \tag{8}$$

Owing to the boundary conditions at $x = ht$ (equations (2b) and (3a)), no constant of integration appears in this equation. By inserting this equation into equation (7a), we have:

$$(v-h)\frac{dr}{dx} = -2v\frac{h-v}{h+v}r^2 + i$$

From the integration of this equation under the condition:

$$\alpha \equiv \left(\frac{i}{2v}\right)\left(\frac{h+v}{h-v}\right) > 0$$

which holds for $h > v$, we have the following solution for r:

$$\left(\frac{h+v}{2v}\right)\left(\frac{1}{2\alpha^{1/2}}\right)\log\left|\frac{r-\alpha^{1/2}}{r+\alpha^{1/2}}\right| = x - ht_0$$

Since it is expected that $0 < r < \alpha^{1/2}$ ($r = 0$ at $x = ht_0$, ad $r \to \alpha^{1/2}$ at $x \neq ht_0$ and $t_0 \to \infty$), we can express the solution as:

$$-\frac{r-\alpha^{1/2}}{r+\alpha^{1/2}} = \exp\left(-\frac{4v\alpha^{1/2}}{h+v}(h-u)t_0\right)$$

where $u \equiv x/t_0$. If the time t_0 is large enough, the solution is approximately:

$$r \sim \alpha^{1/2} = \left[\left(\frac{i}{2v}\right)\left(\frac{h+v}{h-v}\right)\right]^{1/2} \tag{9a}$$

except in the vicinity of the boundary, $u \sim h$. The approximate solution after long times, $t_0 \gg 1$, is considered as the steady-state solution. The steady-state solution for l can be obtained from equations (8) and (9a) except at $u \sim h$:

$$l \sim \left[\left(\frac{i}{2v}\right)\left(\frac{h-v}{h+v}\right)\right]^{1/2} \tag{9b}$$

Region B, $-ht < x < -vt$

Utilizing the symmetry relation of equation (4), the steady-state solutions in this region are determined from those in region A as follows:

$$r \sim \left[\left(\frac{i}{2v}\right)\left(\frac{h-v}{h+v}\right)\right]^{1/2} \tag{10a}$$

$$l \sim \left[\left(\frac{i}{2v}\right)\left(\frac{h+v}{h-v}\right)\right]^{1/2} \tag{10b}$$

Region C, $-vt < x < vt$

We assume that the steady-state solutions in this region are functions of $u \equiv x/t$ only, as Mansfield did[7]:

$$r(x, t) = r(u)$$

$$l(x, t) = l(u)$$

Owing to this assumption, differentials dr and dl are zero on the line $x = ut$, so that we have:

$$\frac{\partial r}{\partial t} + u\frac{\partial r}{\partial x} = 0 \tag{11a}$$

$$\frac{\partial l}{\partial t} + u\frac{\partial l}{\partial x} = 0 \tag{11b}$$

From equations (1) and (11), we obtain:

$$\frac{1}{t_0}(v-u)\frac{dr}{du} = -2vrl + i \tag{12a}$$

$$-\frac{1}{t_0}(v+u)\frac{dl}{du} = -2vrl + i \tag{12b}$$

at a definite time t_0. From the left-hand sides of the equations, we have:

$$(v-u)\frac{dr}{du} = -(v+u)\frac{dl}{du} \tag{13}$$

and these terms can be neglected in equations (12) for the steady state after long times, $t_0 \gg 1$ Then, equations (12) become:

$$2vrl = i \tag{14}$$

From equations (13) and (14), we have:

$$\left[r^2 - \left(\frac{i}{2v}\right)\left(\frac{v+u}{v-u}\right)\right]\frac{dr}{du} = 0$$

and the solutions are:

$$r = \beta \tag{15a}$$

where β is constant, or:

$$r=\left[\left(\frac{i}{2v}\right)\left(\frac{v+u}{v-u}\right)\right]^{1/2} \tag{15b}$$

From equation (14) and solutions (15), the solutions for l are also determined; from the solution (15a):

$$l=\left(\frac{i}{2v}\right)\left(\frac{1}{\beta}\right) \tag{16a}$$

and from the solution (15b):

$$l=\left[\left(\frac{i}{2v}\right)\left(\frac{v-u}{v+u}\right)\right]^{1/2} \tag{16b}$$

Mansfield obtained the solutions (15b) and (16b) from a different analysis[7]. Solutions (15b) and (16b) are not adequate near the boundaries, $x=\pm vt_0$, because the solutions in region C should be continuously connected to the solutions in regions A and B. Solutions (15a) and (16a) satisfy the condition, if the constant β is adjusted. The solutions are identical with solutions (9) near the boundary $x=vt_0$ and solutions (10) near the other boundary $x=-vt_0$. In order to connect these solutions continuously in region C, the solutions should be (15b) and (16b) around the centre $u=0$. Solutions (15b) and (16b) connect with solutions (9) at a certain point x_1 $(=u_1t_0,\ 0<u_1<v)$:

$$u_1=v^2/h \tag{17}$$

and with solutions (10) at the opposite point $-x_1$.

Consequently, we obtain the steady-state solutions of equations (1) subject to the boundary conditions (2) and (3) in the whole range $-ht_0<x<ht_0$: equations (10) for $-ht_0<x<-x_1$, equations (15b) and (16b) for $-x_1<x<x_1$, and equations (9) for $x_1<x<ht_0$. They are shown in *Figure 14* as a function of u. These solutions may be approximate because the derivatives of r and l are not continuous at $u=\pm u_1$. Further studies will be required for the analysis.

The profile of the growth front at time t_0 is given by integrating the differential equation:

$$\mathrm{d}y/\mathrm{d}x=b[l(x,t_0)-r(x,t_0)]$$

where y is the height of the growth front at x, and b is the thickness of a stem. For the solutions for r and l obtained above, the profile becomes part of an ellipse[7] within $-u_1t_0<x<u_1t_0$ and linear outside this region except near $x\sim\pm ht_0$, as shown in *Figure 15*. The schematic shape of the crystal is shown in *Figure 16*. As mentioned earlier for $h>v$, since the width of the $\{1\ 1\ 0\}$ sector does not change, the profile becomes lenticular if the width is narrow enough.

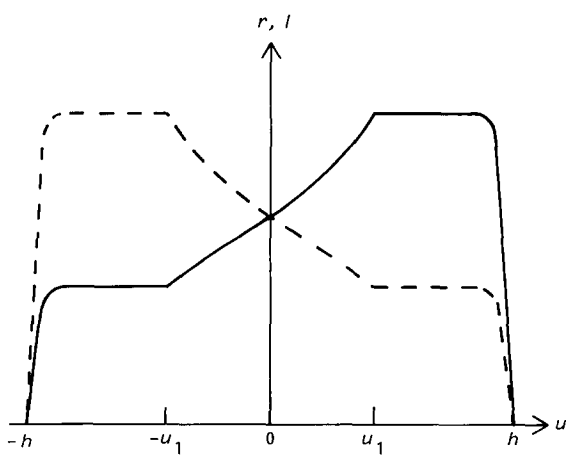

Figure 14 Solutions for r (full curve) and l (broken curve) plotted against u $(=x/t_0)$ for particular values of i, v and h

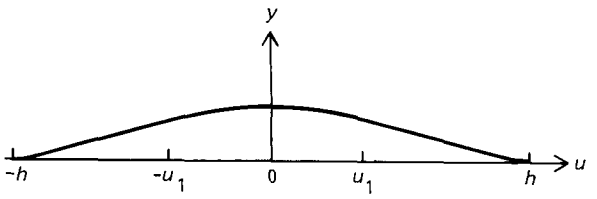

Figure 15 Calculated profile of growth front plotted against u for particular values of i, v and h

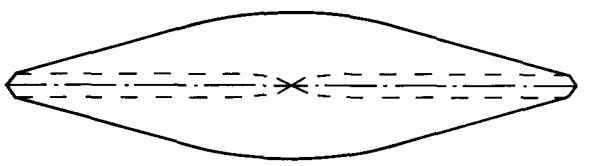

Figure 16 Schematic representation of the profile of a single crystal predicted by the present analysis

The angle 2θ between the lines of the growth front at the tip can be calculated as:

$$\tan\theta=2\left[\left(\frac{ib^2}{2v}\right)\left(\frac{1}{(h/v)^2-1}\right)\right]^{1/2} \tag{18}$$

The growth rate G at the centre of the growth front, $x=0$, can be calculated from the solutions for r and l (equations (15b) and (16b)):

$$G=b[r(0,t_0)+l(0,t_0)]v=b(2iv)^{1/2} \tag{19}$$

With the use of equations (18) and (19), we can express the nucleation rate i and velocity v of steps as a function of h, θ and G:

$$ib^2=\tfrac{1}{2}(G^2/h)\gamma \tag{20}$$

$$v=h/\gamma \tag{21}$$

$$\gamma\equiv\frac{\tan\theta}{[\tan^2\theta-(G/h)^2]^{1/2}} \tag{22}$$

Since these values of h, θ and G were obtained in the present experiments $(G=G_a,\ h=G_b)$, we can determine the rate i and velocity v on a $\{2\ 0\ 0\}$ face from the experimental data, utilizing equations (20)–(22).

APPLICATION OF THE MODEL

Determined rate i and velocity v are plotted in *Figure 17* except for the data with $\tan\theta\sim G/h$ $(=G_a/G_b$: ▲ and △ respectively in *Figures 8* and *10*). It should be noted for such data, i.e. where $\tan\theta\sim G/h$, that i diverges to infinity and v becomes zero because γ diverges to infinity. Since the parameter ib^2/v diverges to infinity for such growth, the growth does not satisfy the condition of nucleation-controlled growth and we cannot apply the present analysis to crystal growth. For the growth, steps have no advantage over a flat surface in crystallization. The outline should be linear because the lateral width of

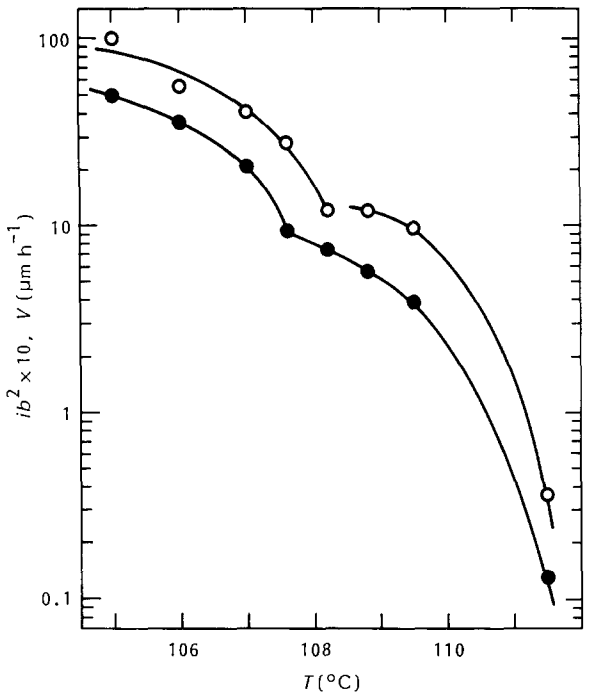

Figure 17 Temperature dependence of ib^2 (●) and v (○) determined from experimental data by the present analysis

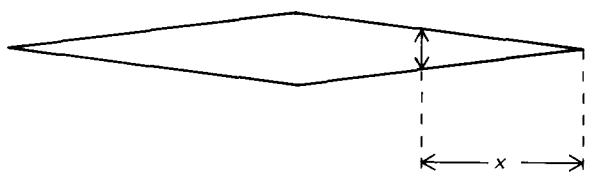

Figure 18 Hypothetical crystal corresponding to $\tan\theta = G/h$. The width is simply proportional to the distance x

crystals is simply proportional to the distance x, as shown in *Figure 18*. *Figure 3c* shows the typical habits for $\tan\theta \sim G/h$; the outlines are actually almost linear except for a narrow central region. From the fact that steps have no advantage in crystallization for the crystals shown in *Figure 3c*, we can expect a strong impurity effect on the steps; the effect will be caused by lower-molecular-weight component in the region crowded with crystals, where these crystals have been observed. The break in the curves of i and v in *Figure 17* derives from the break in growth rate G_a (*Figure 8*) and will be due to the fractionation effect, too.

The strong dependence of v shown in *Figure 17* does not agree with the prediction of standard nucleation theory in which v is expected to show a much weaker dependence on supercooling than i. The strong dependence may be explained as the result of interruption of advancing steps. However, the disagreement may be simply due to the broad distribution of melting points originating in the molecular-weight distribution of the fraction. For the quantitative analysis of the crystallization of low-molecular-weight samples, monodisperse polyethylene will be required.

DISCUSSION

In order to explain curved lateral habits under the condition of nucleation-controlled growth, we must assume the interruption of crystallization on the {2 0 0} face. What causes the interruption? In preceding studies, the following two models have been proposed. (1) An impurity interrupts the advance of steps and reduces the average velocity of steps[6]. By an impurity we mean inclusion, branching, lower-molecular-weight component or solvent used for solution growth. We also include, among impurities, self-poisoning on the steps of extended-chain crystals by the stem of a once-folded chain[22]. (2) Owing to lattice strain caused by chain folding, crystallization becomes slower because the free energy of the crystals increases[8]. In both models, the authors explained the difference in the profile of the growth front between {1 1 0} and {2 0 0} sectors and the anisotropy of habits as the result of anisotropy of orthorhombic crystal structure of polyethylene, namely as the result of distinct structures of steps or chain folding between the {1 1 0} and {2 0 0} sectors.

We can rule out the possibility that the lattice strain caused by chain folding is the main reason for curved habits because rounded lateral habits have been observed for not only folded-chain but also extended-chain crystals, as shown in the present experiment; similar habits of extended-chain crystals were also observed with monodisperse low-molecular-weight polyethylene[23]. It can also be said from the evidence of curved habits of monodisperse polyethylene that the impurity effect caused by low-molecular-weight component will not be the main reason; but the effect cannot be neglected at low supercoolings for the present samples with molecular-weight distribution. The effect of solvent will be negligible for the melt crystallization of curved single crystals[10–13]. Self-poisoning may play an important role in the crystallization of extended-chain crystals[22], but the effect will not be expected for the crystallization of chain-folded crystals of higher-molecular-weight polyethylene. Therefore, the effects (1) and (2) listed above will not be the main reason for the interrupted advance of steps on the {2 0 0} face and the resultant curved habits.

As another possibility, defects in crystals are supposed to be obstacles for the advance of steps. Although the degree of disorder in crystals has not been well studied at higher temperatures where the crystallization occurs ($T > 100$°C), it is possible that polyethylene crystals are considerably disordered near the melting point in the same way as alkane crystals; tilting of chains in the crystals supports the hypothesis, as was discussed in the section on 'Experiments and results'. In the disordered state, crystals may be divided into small coherent domains several nanometres wide with distinct stacking, as was predicted by Monte Carlo simulation[24]; the boundaries of these domains form stacking faults. The average velocity of steps will be reduced by the boundaries appearing on the growth front. The anisotropy of the habits can be explained if the excess energy required for crossing the boundaries on a {2 0 0} face is larger than the energy on a {1 1 0} face. We must examine these speculations on the defects in crystals experimentally.

For simplicity, we assumed a continuous substrate in the theoretical calculations of the kinetic model. We can obtain any large angle, 2θ, up to 180° at the tips of the calculated profile; θ becomes larger with decreasing $|v - h|$ and is 90° at $v = h$. However, for the {2 0 0} face of polyethylene, since the angle at a step is the angle

between ⟨0 1 0⟩ and ⟨1 1 0⟩ directions, θ_0 ($\sim 56°$), we cannot construct habits whose tips are at an angle larger than $2\theta_0$. Therefore, for $v \sim h$, the calculation becomes incorrect and we must take into consideration the discreteness of the crystal lattice for $\theta \sim \theta_0$. In the present experiments, θ is smaller than 30° in all cases examined, so that we can neglect the effect of discreteness.

CONCLUSIONS

Single crystals of low-molecular-weight polyethylene ($M_w = 2000$ and $M_w/M_n = 1.1$) show different kinds of morphology from those of higher-molecular-weight polyethylene, in crystallization from n-hexacontane solution at high temperatures ($T > 105$°C). The shape of the crystals is lenticular; the profile is curved in the central region and almost linear near the tips, where the outline has an acute angle. In this habit, the {1 1 0} growth face disappears. Most chains are extended in these crystals and inclined in the direction of the a axis; the sense of the chain tilting is identical in a whole crystal. From the decoration pattern of evaporated polyethylene on a lamellar surface, it is supposed that the surface is rather disordered in comparison with alkane single crystals. Enhanced growth has been recognized at the re-entrant corner of {3 1 0} twins and this fact gives strong evidence for nucleation-controlled growth on normal faces. A linear growth rate of single crystals has been obtained for both directions of a and b axes. The growth rates show an exponential dependence on crystallization temperature. The dissolution temperature was not determined because the sample has a molecular-weight distribution that broadens the dissolution temperature of the low-molecular-weight fraction strongly.

The growth of single crystals has been analysed with the kinetic theory of Seto and Frank on the basis of nucleation-controlled growth. For moving boundaries of growth sector, retardation of advance of steps results in the curved profile of the growth front, as was suggested by Mansfield. In the present analysis, it has been shown that lenticular habits can be expected when the velocity of advancing steps on the {2 0 0} face becomes lower than that of moving sector boundaries. From the analysis, we have obtained equations with which the nucleation rate and velocity of steps on the {2 0 0} face can be determined from the experimental data of growth rates along a and b axes and the angles at the tips of lenticular crystals. The determined nucleation rate and velocity of steps show exponential dependence on crystallization temperature. The dependence of the velocity of steps does not agree with the prediction of standard nucleation theory and may be experimental evidence for the interrupted advance on a {2 0 0} face. However, the disagreement may be simply due to the broad distribution of melting points of the sample. For quantitative analysis, monodisperse polyethylene will be required.

We can rule out the possibility that the lattice strain caused by chain folding is the main reason for curved habits because not only folded-chain but also extended-chain crystals show rounded habits. The effect of impurity will not be the main reason, either, because it has been reported that monodisperse polyethylene also shows curved habits. Defects appearing on the growth face can be the main reason for curved habits, namely the cause of retarded advance of steps; crystals will be rather disordered at high temperatures and the defects may be formed by the boundaries of small domains with distinct stacking. Further studies should be required in order to clarify the reason for the interruption of advance of steps on the {2 0 0} face.

ACKNOWLEDGEMENTS

I would like to thank Professor H. Kiho and Drs H. Miyaji, K. Izumi and Y. Miyamoto (Kyoto University) for their valuable discussions. This work was partly supported by a Grant-in-Aid for Scientific Research from the Ministry of Education, Science and Culture.

REFERENCES

1 Geil, P. H. 'Polymer Single Crystals', Wiley, New York, 1963
2 Khoury, F. and Passaglia, E. 'Treatise on Solid State Chemistry' (Ed. N. B. Hannay), Plenum, New York, 1976, Vol. 3, Ch. 7
3 Khoury, F. *Polym. Prepr. Japan* 1982, **31**, 5
4 Organ, S. J. and Keller, A. *J. Mater. Sci.* 1985, **20**, 1571
5 Sadler, D. M. *Polymer* 1983, **24**, 1401
6 Toda, A. *J. Phys. Soc. Japan* 1986, **55**, 3419
7 Mansfield, M. L. *Polymer* 1988, **29**, 1755
8 Hoffman, J. D. and Miller, R. L. *Macromolecules* 1989, **22**, 3038
9 van Beijeren, H. and Nolden, I. 'Structure and Dynamics of Surfaces II', Topics in Current Physics (Eds. W. Schommers and P. von Blanckenhagen), Springer, Berlin, 1987, Vol. 43, Ch. 7
10 Hikosaka, M. and Seto, T. *Japan. J. Appl. Phys.* 1982, **21**, L332
11 Bassett, D. C., Olley, R. H. and Al Raheil, I. A. M. *Polymer* 1988, **29**, 1539
12 Labaig, J. J. Ph.D. Thesis, Strasbourg, 1978
13 Keith, H. D., Padden, F. J. Jr, Lotz, B. and Wittmann, J. C. *Macromolecules* 1989, **22**, 2230
14 Khoury, F. *Faraday Disc. Chem. Soc.* 1979, **68**, 404
15 Ewen, B., Strobl, G. R. and Richter, D. *Faraday Disc. Chem. Soc.* 1980, **69**, 19
16 Wittmann, J. C. and Lotz, B. *J. Polym. Sci., Polym. Phys. Edn.* 1985, **23**, 205
17 Blundell, D. J., Keller, A. and Kovacs, A. J. *J. Polym. Sci. (B)* 1966, **4**, 481
18 Prasad, A. and Mandelkern, L. *Macromolecules* 1989, **22**, 914
19 Hikosaka, M. *Polymer* 1987, **28**, 1257
20 Seto, T. *Rep. Prog. Polym. Phys. Japan* 1964, **7**, 67
21 Frank, F. C. *J. Cryst. Growth* 1974, **22**, 233
22 Ungar, G. and Keller, A. *Polymer* 1987, **28**, 1899
23 Hikosaka, M. and Ungar, G. private communication
24 Yamamoto, T. *J. Chem. Phys.* 1988, **89**, 2356

Note added in proof

At the 33rd IUPAC International Symposium on Macromolecules, Montreal, 8–13 July 1990, Professor Point independently presented the strict solution for the shape of lenticular crystals. The solution can be approximately expressed as part of an ellipse and two straight segments tangent to the ellipse; the approximate solution of the present analysis is justified.